A Lower Troposphere Radar: 1.3-GHz Active Phased-Array Type Wind Profiler with RASS

Hiroyuki HASHIGUCHI, Shoichiro FUKAO, Yuki MORITANI[1]

Research Institute for Sustainable Humanosphere,[2] *Kyoto University, Kyoto, Japan*

Toshio WAKAYAMA and Shinichiro WATANABE

Mitsubishi Electric Corporation, Amagasaki, Japan

(Manuscript received 16 May 2001, in final form 4 March 2004)

Abstract

We have developed an atmospheric radar (wind profiler) for lower tropospheric observations (Lower Troposphere Radar: LTR), based on the 1357.5-MHz boundary layer radar (BLR), which we previously developed mainly for observations of the atmospheric boundary layer. System gain of this radar is improved due to newly developed large-sized active phased-array antenna, active transmitting modules with higher output power, and pulse compression technique. It has the following functions: an antenna gain of 33 dBi is obtained with a 4 m $\times$ 4 m active phased array antenna which has 96 antenna subelements, a peak output power of 2 kW is obtained by 24 active transmitting modules, and maximum S/N is improved 8 times by using a pulse compression technique which uses 8-bit optimized coding developed by Spano and Ghebrebrhan (1996c). The LTR is the first active phased-array 1.3 GHz-band wind profiler radar. It is possible to vary the beam direction by electronically steering the zenith angle within 45°. Atmospheric winds in the lower troposphere, including the atmospheric boundary layer, are obtained with high time and height resolutions in real time. Observations of atmospheric temperature are also possible using the radio acoustic sounding system (RASS) technique with speaker horns. We have confirmed LTR's potential as a reliable tool for atmospheric observations, using simultaneous observation results with the MU (Middle and Upper atmosphere) radar, a Doppler sodar, and a radiosonde.

1. Introduction

Observations of wind velocity profiles are very important for studying meteorological phenomena, weather forecasting etc. An atmospheric radar (wind profiler) is one of the most suitable remote sensing instruments for observing height profiles of three components of wind velocity vector, including the vertical velocity, with high time and height resolutions without influence of weather conditions. A small-sized 915-MHz boundary layer radar (BLR), using microstrip antenna technology to observe the wind velocities in the atmospheric boundary layer (ABL), was first developed by Ecklund et al. (1988, 1990) at Aeronomy Laboratory of NOAA (National Oceanic and Atmospheric Administration) in the United States. The 915-MHz BLRs, which have been dealt in by a commercial vendor in the United States, have become very popular in recent years and have been found to be very effective for studies of the first few kilometers of the atmosphere. Carter et al. (1995) provides a good review of 915-MHz BLRs.

Corresponding author: Hiroyuki Hashiguchi, Research Institute for Sustainable Humanosphere, Kyoto University, Uji, Kyoto 611-0011, Japan.
E-mail: hasiguti@rish.kyoto-u.ac.jp
1 Present affiliation: NTT DoCoMo
2 RISH was reorganized from Radio Science Center for Space and Atmosphere (RASC) on April 1, 2004.

RASC (Radio Science Center for Space and Atmosphere of Kyoto University) group independently developed a 1357.5-MHz BLR in 1992 (hereafter referred to as 1.3-GHz BLR, or simply BLR) (Hashiguchi et al. 1995a). It has three parabolic antennas with a diameter of 2 m and a peak output power of 1 kW. Atmospheric observations have been continuously conducted since 1992 at Serpong (6.4°S, 106.7°E), situated in the southwest suburbs of Jakarta in Indonesia. It has been providing valuable information on active convection and unstable structures of the moist atmosphere in the equatorial region (Hashiguchi et al. 1995b, c, 1996, 1997; Tsuda et al. 1995; Widiyatmi et al. 1999, 2001; Hadi et al. 2000). CRL (Communication Research Laboratory) group independently developed a 1357.5-MHz BLR system, which is used in continuous observations in Japan and India (Ohno 1995; Reddy et al. 2000).

Although an atmospheric radar to easily observe the whole important region in the lower troposphere has become necessary in recent years, ordinary BLRs for observing the ABL are insufficient for this purpose. Commercially, a 400-MHz wind profiler to observe the whole lower troposphere can be purchased from a vendor in the United States. One, for example, is installed at the Meteorological Research Institute at Tsukuba in Japan. It has, however, a relatively large antenna and lacks transportability. We have developed a 1357.5-MHz Lower Troposphere Radar (hereafter referred to as 1.3-GHz LTR, or simply LTR) for enabling observations of height profiles of wind velocity in the whole lower troposphere. It combines the advantage of the transportability of the 1.3-GHz BLR with enlarged observable height range. The radar has a peak output power of 2 kW with a $4\ \mathrm{m} \times 4\ \mathrm{m}$ active phased array antenna which can be divided into the quadrisection for comparatively easy transportability. This is the first active phased-array 1.3-GHz band wind profiler radar. It also enables observations of atmospheric temperature using the radio acoustic sounding system (RASS) technique with speaker horns (e.g., Adachi et al. 1993; May et al. 1996). The same radar system is adopted in the wind profiler network, the Wind Profiler Data Acquisition System (WINDAS), of the Japan Meteorological Agency (JMA) (Ishihara and Goda 2000; Kato et al. 2004).

This paper presents a system design including RASS and initial observational results of the LTR. In Section 2, we describe a system design of the LTR. In Sections 3 and 4, we describe details of the hardware and software subsystems, respectively. In Section 5, we describe initial observational results of the LTR, including the comparison with the wind velocities simultaneously observed by the MU radar and a Doppler sodar. In Section 6, we describe the development of LTR/RASS, and the comparison of a temperature profile with radiosonde sounding. Finally, we present our conclusions in Section 7.

2. System design

We have developed the LTR to observe the whole lower troposphere by enlarging the 1.3-GHz BLR, but preserving its transportability. The LTR has been designed to meet the following requirements:

1. The system should be transportable and relatively inexpensive for widespread utilization.
2. The system should have a range resolution of 100 m or better, and a time resolution of 1 min or better.
3. System recovery should be fast enough to obtain useful data at height as low as 200 m.
4. The LTR should be sensitive enough to observe height profiles of three components of wind velocity vector up to the height of at least 5–6 km to cover the whole lower troposphere under typical atmospheric conditions.
5. The LTR should be able to measure height profiles of temperature by RASS observations in the ABL.
6. The LTR should be able to change beam zenith angles for RASS observations.

In order to reduce system recovery time (i.e., to make the minimum observable height lower), the operational frequency of the LTR must be higher than that of VHF atmospheric radars. Since 1357.5 MHz is allocated for this type of radars by the Japanese government, we decided to use the same frequency as the 1.3-GHz BLR.

We decided to use an active phased array antenna for the LTR for the following reasons:

1. It can perform fast beam steering to chase RASS acoustic wave.
2. It can obtain a high duty ratio by dividing transmitters to obtain high average output power.
3. It is relatively light in weight for ease of transportability.

We decided to use a 4 m × 4 m phased array antenna, which is relatively large to be able to observe the whole lower troposphere. We made the antenna dividable into quadrisection for ease of transportability. Although we adopted the active phased array antenna, of which the antenna aperture was five times as large as the 1.3-GHz BLR using three parabolic antennas, the necessary space for the installation hardly changes. It is known from experience that the ground clutter echoes can be suppressed when the radiation point is below approximately one radar wavelength λ (22 cm for the LTR) from the ground. We therefore made the antenna plane lower than 20 cm. The far field of the LTR, which is given by D^2/λ (where D is the diameter of the antenna), is about 70 m, that is enough to obtain data from the 200 m range. The antenna beam can be electronically steered vertically and in four oblique directions (usually along north, south, east, and west while depending on antenna arrangement) within any zenith angle of 45° (Adachi and Kobayashi 2001).

In order to observe the whole lower troposphere, we decided 2 kW for a peak output power, which is twice as large as the 1.3-GHz BLR, and to use pulse compression techniques by which signal-to-noise ratio (S/N) can be improved without deteriorating the range resolution. S/N becomes N times as strong as that of a single pulse transmission with N bit pulse compression. There are several methods for pulse compression, but binary phase-coded pulse compression is most practical. In this method, a transmitted pulse is equally divided into N parts, and each part is modulated to have a phase of 0° or 180°. The received signal is demodulated by calculating a correlation with the transmitted pulse sequence. As the code for the binary phase-coded pulse compression, Barker and complementary codes are well-known (e.g., Schmidt et al. 1979; Woodman 1980). Best complementary code for decoding sampling data in the truncated range was shown by Spano and Ghebrebrhan (1996a, b, c). They examined the best complementary code pair for suppressing sidelobes due to the imperfection of transmitted pulses and echoes from undesired directions.

Table 1. Specifications of the LTR system.

Radar system:	Monostatic pulse Doppler radar
Operational frequency:	1357.5 MHz
Antenna:	Phased array antenna
Aperture:	4 m × 4 m
Beam width:	4.0° (half power)
Beam direction:	zenith, north, south, east, and west
Beam angle:	variable (0°–45° of zenith)
Gain:	33 dBi
Transmitter:	
Peak power:	2 kW
Average power:	428 W (duty ratio 21.4%) (maximum)
Bandwidth:	10 MHz
Pulselength:	0.67, 1.00, 1.33 μs (variable)
IPP:	25, 50, 100 μs (variable)
Receiver:	
Form:	Double super heterodyne
Output signal:	I and Q video
Bandwidth:	1.8, 1.2, 0.9 MHz (variable)
Data acquisition unit:	
Interface:	100 BaseT

3. System configuration

Table 1 shows the specifications of the LTR system. To satisfy the requirement for the range resolution, we enabled a sub-pulse width of 0.67 μs, corresponding to a range resolution of 100 m. It is possible to change the zenith angle of beam direction for the RASS observations.

The hardware system of the LTR consists of five parts, which are a phased array antenna, an active module unit, a transmitter/receiver unit, a data acquisition unit, and a signal processing unit. Figure 1 shows the block diagram of the LTR system. First we describe the signal flow during an observation. The radio frequency (RF) signal generated in the transmitter unit is phase-shifted and amplified in the module unit, and radiated from the antenna.

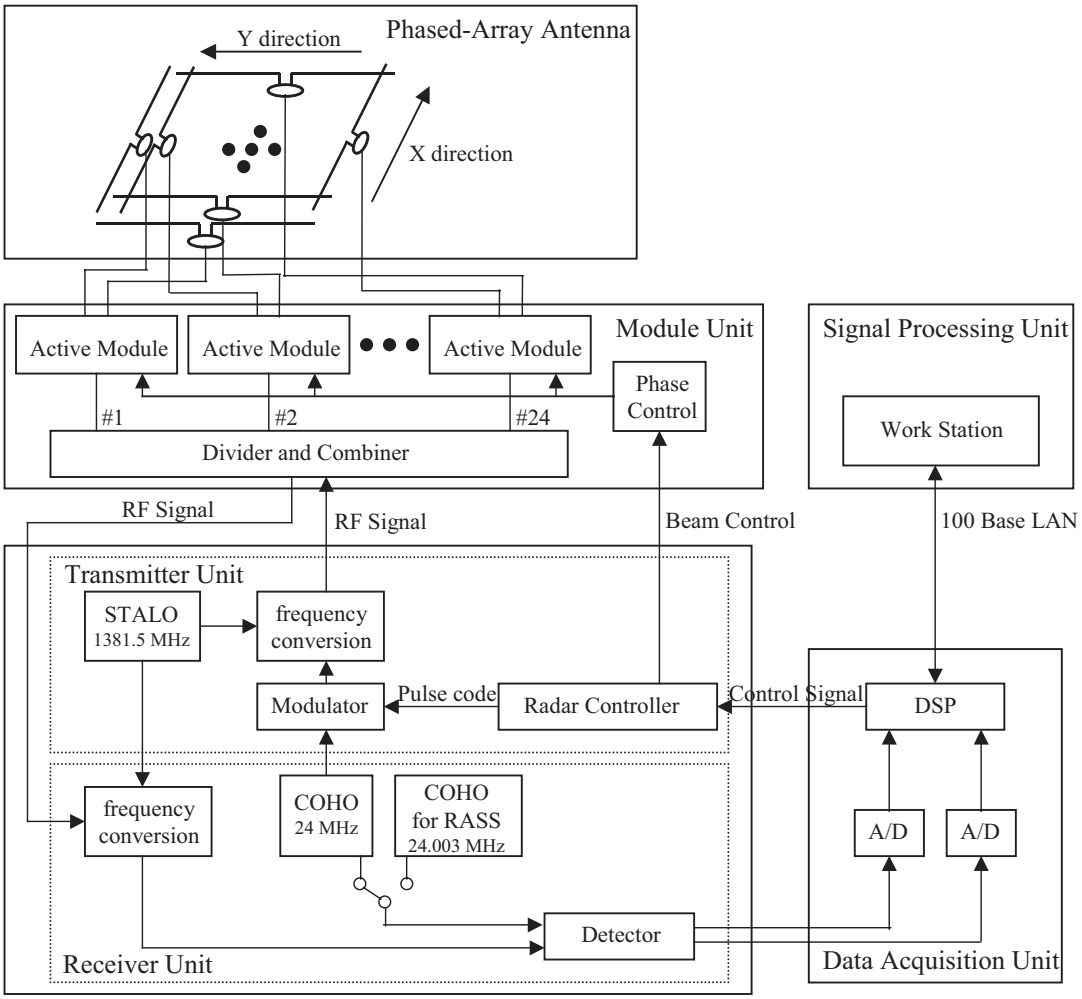

Fig. 1. Schemaric block diagram of the LTR system. STALO and COHO are the abbreviation of stable local oscillator and coherent oscillator, respectively.

Then the antenna gathers the signal scattered by atmospheric turbulence and transfers it to the module unit. The received signal is amplified in the module unit and detected in the receiver unit. Thereafter, the signal is converted to a digital signal, which is decoded and integrated in the data acquisition unit. The data acquisition unit transfers the signal to the signal processing unit. Finally, some calculations are performed in the signal processing unit. The detailed description of each unit will be presented in the following subsections.

3.1 Active phased array antenna

Figure 2 shows the outlook of the LTR and its antenna elements. An electromagnetic coupling coaxial dipole (ECCD) antenna, which was originally developed for using the base station of the Personal Handy-phone System (PHS), is used as the antenna element (Miyashita et al. 1999). This antenna element is impervious to water. To reduce the ground clutter echoes, the height of the radiation point is chosen about 20 cm, while that of the 1.3-GHz BLR was about 1.5 m. The physical arrangement of the antenna is 24 rows (x direction) and 24 columns (y direction) of elements, each of which is sub-divided into 2 sub-elements. A total of 96 sub-elements (that is 24×2 $(x, y) \times 2$ distribution) are used. The active module is connected to four sub-elements through distributors in such a way that a module controls

(a)

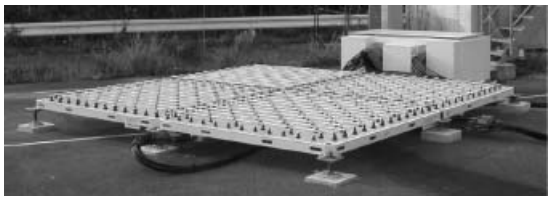

(b)

Fig. 2. Pictures of (a) the LTR and (b) the antenna elements.

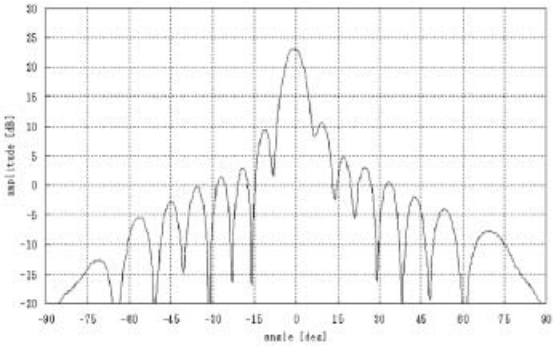

Fig. 3. Measured antenna pattern of the LTR.

two sub-elements each for one row and one column. The antenna can be divided into four sub-antennas. It is possible to operate the radar using one sub-antenna (whose size is 2 m $\times$ 2 m) for utilization in a relatively small installation space, although the power-aperture product becomes 1/8 compared with the original configuration. The weight of one sub-antenna is about 60 kg so that it can be moved by a few persons. By controlling the phase of the phase shifter connected for x (y) direction antenna elements, we can steer the beam in the x (y) direction. Although it is possible to steer the beam only along the x and y directions, it is possible to electronically fast change the zenith angle within 45° in 0.7° steps. No grating lobe appears within 15°. The half power beamwidth and the antenna gain are 4.0° and 33 dBi, respectively. Figure 3 shows the measured antenna pattern.

3.2 Module and transmitter/receiver units

The module unit has 24 active modules. One module corresponds to two antenna sub-elements each for x and y directions, and selects x or y direction according to the beam direction. In transmission, the RF signal from the transmitter unit is divided, amplified, and transferred to the antenna elements. In reception, the weak received signals from the antenna elements are amplified, combined, and transferred to the receiver unit. Circulators and PIN-diode switches in the active modules are used for the transmitting/receiving switch. The phase of transmitting RF signals is also controlled in the active modules having 5-bit phase shifter, and the phases of transmission and reception are controlled independently. The module unit is placed in the vicinity of the antenna in order to reduce the cable loss.

The transmitter unit is composed of a stable local oscillator (STALO) of 1381.5 MHz, a frequency conversion unit, a modulator, and a radar controller. The IF (intermediate frequency) transmitted source signal of 24 MHz is generated by applying a specified phase-modulation and pulse-modulation to the COHO (coherent oscillator) signal in the modulator. The source signal is up-converted to the RF transmitted signal of 1357.5 MHz by mixing it with the STALO signal in the frequency conversion unit. The RF signal is then sent to the module unit.

The receiver unit is composed of two COHOs of 24 MHz and 24.003 MHz, a frequency conversion unit (which forms a super-heterodyne receiver), and a phase detector. The signal received at 1357.5 MHz is down-converted to the IF of 24 MHz in the frequency conversion unit. The IF signal is subsequently down-converted to a video signal (analog signal) by the COHO,

and into in-phase (I) and quadrature-phase (Q) signals by a phase detector. In the case of the RASS mode, the center frequency of the I and Q video signals is shifted by 3 kHz with respect to the normal mode, in order to detect the acoustic line spectra (see Section 6 for details). The video signal is transferred to the analogue-to-digital converter (A/D) in the data acquisition unit.

3.3 Data acquisition and signal processing units

The data acquisition unit consists of two A/Ds and DSP (Digital Signal Processor) unit. The I and Q video signals are converted to 14-bit digital signals in the A/D. The sampling interval is equal to the sub-pulse width. In the DSP unit, the digital signal is decoded according to the pulse compression code, and a number of digital signals are coherently integrated. Then the digital signals are transferred to the signal processing unit.

The LTR system uses an engineering workstation as the signal processing unit. The operating system is UNIX, which is a popular multi-user and multi-task operating system. The workstation can execute some calculations such as fast Fourier transform (FFT) up to 4096-points, incoherent integrations, and estimation of spectral parameters. Because it is necessary to realize the high speed and large data transfer, the private LAN (local area network) of 100 baseT is used as a interface between the data acquisition unit and the signal processing unit. All parameters to control the LTR system, and the observed data transferred from the data acquisition unit, are transferred through this network.

4. Software system

The software to control observations and to process data must have the performance to utilize the hardware of the LTR. The operators control the entire LTR system by using only the observation software. The observation software of the workstation should have the following functions:

1. A function to set up observation parameters and to control observations.
2. A function to transfer data from the data acquisition unit to the workstation and to send parameters to the LTR.

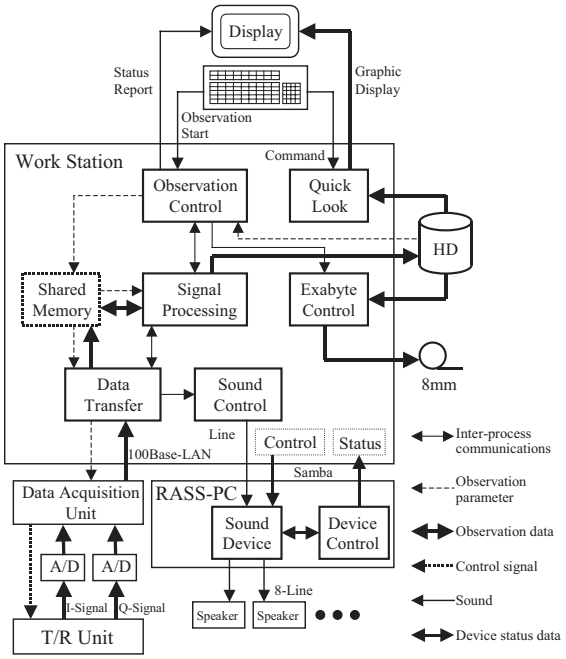

Fig. 4. Block diagram of the observation software including the RASS observations (see Section 6 for RASS).

3. A function to process the data—FFT, incoherent integrations, the estimation of spectral parameters, and so on.
4. A function to record data onto an 8 mm tape.
5. A function to graphically display the observation data simultaneously with the observation.

Figure 4 shows the block diagram of the observation software in the workstation. Note that this figure includes the software for RASS observations which will be described in Section 6. The observation software includes programs named 'Observation Control', 'Signal Processing', 'Data Transfer', 'Exabyte Control', and 'Quick Look'. 'T/R Unit' in this figure indicates the whole system except for the data acquisition unit and the workstation. The 'Observation Control' program's functions are to set up observation parameters and to control the whole observations. The 'Data Transfer' program's functions are to transfer data from the data acquisition unit to the workstation and to send parameters to 'T/R Unit'. The 'Signal Processing' program's functions are to perform signal processing such as FFT, incoherent integrations, to estimate the spectral parameters from

the data taken by the 'Data Transfer' program, and to write observed results to the hard disk (HD). The 'Exabyte Control' program's function is to record the data onto an 8 mm tape from the hard disk without interrupting the observation. The 'Quick Look' program's function is to display the observation data to the display of the workstation and/or of other computer systems even during the observation.

These programs must be operated in parallel and be executed easily by the operators. Therefore, we utilize the multi-task function in UNIX. The observation data are taken by the 'Data Transfer' program and used by the 'Signal Processing' program. Therefore, it is also necessary to deliver the data from the 'Data Transfer' program to the 'Signal Processing' program. For this communication, we use the inter-process communication, which is called 'shared-memory'. Usually, separated programs cannot access the same memory address in UNIX. The 'shared memory' provides the function to access the same memory address from separated programs. On the other hand, it is expected that shared-memory conflict will occur, because the shared-memory is used by two programs. To avoid this conflict, we use the synchronous mechanism, which is called 'semaphore'.

When we start an observation, the 'Observation Control' program should be executed. The file name of the observation parameters, the observation start time, and observation end time or the number of the observations can be specified. The 'Observation Control' program initializes the shared-memory, writes the parameters into the shared-memory, and opens the sockets of the LAN communication with the data acquisition unit. Then the 'Observation Control' program executes the 'Data Transfer' program automatically, and sleeps until the 'Data Transfer' has completed executing. The 'Data Transfer' program initializes the semaphore, executes the 'Signal Processing' program automatically, and 'Signal Processing' program waits until the 'Data Transfer' program resets the semaphore. The 'Data Transfer' program reads the parameters from the shared-memory and sends the parameters to 'T/R Unit' through the socket for the radar control.

The 'Data Transfer' program sends the control signal to start observation to 'T/R Unit' through the data acquisition unit, and then the observation is started. Afterwards, the 'Data Transfer' program waits for the data to become ready. After an observation corresponding to one beam is over, the data acquisition unit transfers the observation data through the socket. Then the 'Data Transfer' program sets the semaphore to prevent access to the shared-memory by 'Signal Processing', and transfers the data into the shared-memory. When the 'Data Transfer' program takes and writes the data for all beams, the 'Data Transfer' program resets the semaphore. Then the 'Signal Processing' program starts the calculations of FFT and incoherent integrations. When the specified incoherent integrations have been performed, the 'Signal Processing' program performs the estimation of spectral parameters, which consists of noise level, peak power, mean Doppler shift, and spectral width. When the estimation of spectral parameters for all beams is finished, the 'Signal Processing' program writes the data onto the hard disk. The 'Data Transfer' program starts the next observation without waiting for the end of the calculations by the 'Signal Processing' program.

When it reaches the specified observation end time or last observation, the 'Data Transfer' and 'Signal Processing' terminate. Then, the 'Observation Control' program executes the 'Exabyte Control' program and exits without waiting for the end of 'Exabyte Control' program. The 'Exabyte Control' program reads the data recorded in the hard disk and writes them onto an 8 mm tape. The 'Quick Look' program reads observed data from the hard disk and graphically displays it.

5. Experiments at the Shigaraki MU Observatory

The LTR was installed at the Shigaraki MU Observatory (34.85°N, 136.10°E, 385 m above sea level) in February, 1999. The LTR was operated for system checks during March–April 1999, and has been continuously operated since May 1999. In this section, we evaluate the performance of the LTR system, based on the simultaneous observations with the MU radar (Fukao et al. 1985a, b) and the Doppler sodar (Ito 1997). We also present preliminary observational results of wind variations associated with the typhoon passage.

Table 2. Observation parameters of the LTR and the MU radar on June 24–July 9, 2000.

Parameter	The LTR	The MU radar
Inter-pulse period (IPP):	100 μs	400 μs
Sub-pulse width:	1.00 μs	1.00 μs
Number of coherent integrations:	32	38
Number of FFT points:	128	128
Number of incoherent integrations:	30	5
Number of sampling points:	64	128
Number of sub-pulses:	8	1
Number of beam direction:	5	5
Zenith angle:	9.8°	10°

5.1 *Simultaneous measurements with the MU radar and a Doppler sodar*

It is known that the MU radar can provide reliable wind velocity data above 1.5 km in height. In order to evaluate the accuracy of the data obtained by the LTR, we compare the observation data of the LTR with those of the MU radar. We conducted simultaneous observations with the MU radar on June 24–July 9, 2000. The MU radar was operated in the tropospheric standard observation mode (Fukao et al. 1990), and the LTR is operated in 8-bit pulse compression mode. The observation parameters of the LTR and the MU radar are shown in Table 2. The observation parameters of the LTR were chosen to sample the data up to a height of about 10 km. The IPP was 100 μs, the sub-pulse width was 1.0 μs (corresponding to range resolution of 150 m), and the number of sampling points was 64. Figure 5 shows the height profiles of the wind velocities obtained by the LTR and the MU radar, averaged over 0830–0930 LT on July 2, 2000 in clear conditions. All of the components of the wind velocities are in good agreement between the two radars in the height range of 1.5–5.0 km. In this case, there was no rain so that the vertical component is also in good agreement between the two radars. The sensitivity to precipitation is proportional to the fourth power of the radar frequency, so that the LTR has approximately 60 dB higher sensitivity to precipitation than to atmospheric turbulence under typical conditions. Therefore, in the rainy case, the LTR can

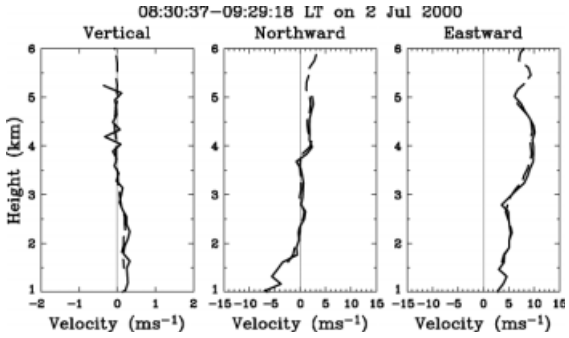

Fig. 5. Height profiles of wind velocities averaged over 0830–0930 LT on July 2, 2000. The solid and dashed curves show the profiles observed by the LTR and the MU radar, respectively. The left, center, and right panels show vertical, northward, and eastward components, respectively.

obtain the precipitation echoes in higher altitudes than the clear-air echoes, but cannot provide the atmospheric vertical motion. Note that the LTR can provide the horizontal winds even in the rainy period, since it is known that the horizontal motion of the precipitation is identical to the atmospheric motion (Fukao et al. 1985c; Wakasugi et al. 1986, 1987). Figure 6 shows the scatter plot of horizontal winds obtained with the LTR and the MU radar, averaged every one hour during June 24–July 9, 2000. The data used for the comparison are in

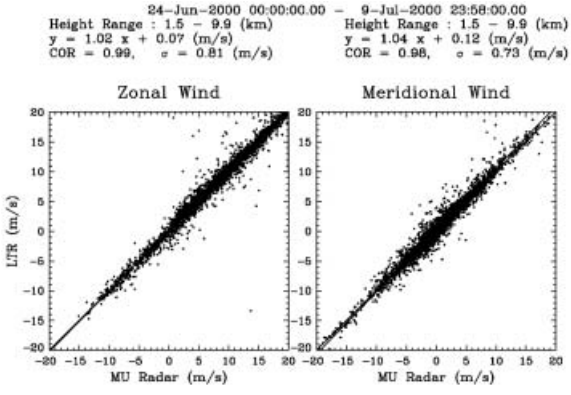

Fig. 6. Scatter plot of zonal (left panel) and meridional (right panel) wind velocities observed with the LTR and the MU radar during June 24–July 9, 2000.

Table 3. Observation parameters of the LTR and the Doppler sodar on December 2, 1999.

Parameter	The LTR	The Doppler sodar
Inter-pulse period (IPP):	50 μs	6 s
Sub-pulse width:	0.67 μs	200 ms
Number of coherent integrations:	64	none
Number of FFT points:	128	64
Number of incoherent integrations:	30	none
Number of sampling points:	30	16
Number of sub-pulses:	1	1
Number of beam direction:	5	5
Zenith angle:	9.8°	20°

all time including rainy period and in all height range, where effective data are obtained with both radars. The wind velocities are in good agreement between the two radars. We have not shown the similar diagram for the vertical component, because the vertical wind profile of the LTR is different from that of the MU radar in the rainy period due to the above-mentioned reason.

We also conducted the observations with a Doppler sodar on December 2, 1999, to examine the lowest observable height. The Doppler sodar has the operating frequency of 2.1 kHz and is known to provide the reliable data from 50 m up to about 500 m heights (Gaynor 1994). The parameters of the LTR and the Doppler sodar are shown in Table 3. We chose the observation parameters of the LTR to observe at the lowest possible height range. The IPP was 50 μs, the sub-pulse width was 0.67 μs (corresponding to the range resolution of 100 m), and no pulse compression mode was used. We compare the averaged height profiles of the wind velocities obtained by the LTR with those obtained by the Doppler sodar, as shown in Fig. 7. Since there was weak rain, the vertical component of the LTR is much larger than that of the Doppler sodar below 0.4 km. Northward and eastward components give a comparably good agreement from the lowest observation height of 195 m. We conclude the LTR satisfies the requirement of the lowest observable height of 200 m.

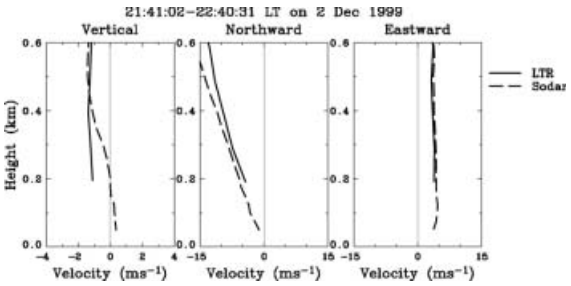

Fig. 7. Height profiles of wind velocities averaged over 2130–2230 LT on December 2, 1999. The solid and dashed curves show the profiles observed by the LTR and the Doppler sodar, respectively.

5.2 *Evaluation of pulse compression*

The LTR usually uses Spano and Ghebrebrhan's optimized codes for 4-bit and 8-bit pulse compression. To evaluate the effect of the pulse compression, we operated the LTR by interlacing three observation modes, (a single-pulse, a 4-bit pulse compression, and an 8-bit pulse compression mode) on June 19, 1999. Table 4 shows the observation parameters. We used the same parameters for the three observation modes except for the pulse compression mode. Figure 8 shows the height profiles of averaged signal-to-noise ratio (S/N) for single pulse, 4-bit pulse compression, and 8-bit pulse compression in the rainy period during 0130–0330 LT on June 19, 1999. The S/N of 4-bit pulse compression is much larger than that of single-pulse, and that of 8-bit pulse compression is even larger. The effects of the pulse compression are well shown.

Table 4. Observation parameters of the LTR on June 19, 1999.

Parameter	Value
Inter-pulse period (IPP):	100 μs
Sub-pulse width:	1.00 μs
Number of coherent integrations:	64
Number of FFT points:	128
Number of incoherent integrations:	30
Number of sampling points:	64
Number of beam direction:	5
Zenith angle:	9.8°

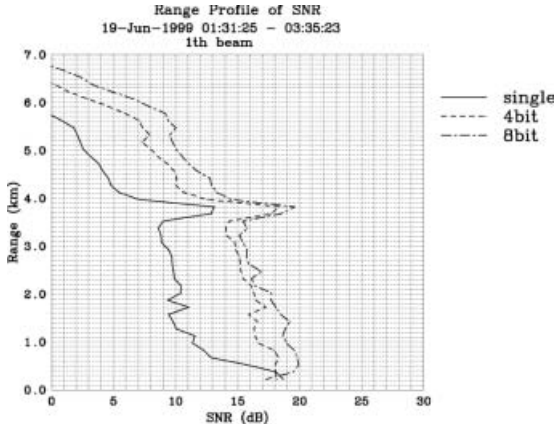

Fig. 8. Height profiles of averaged signal-to-noise ratio for single pulse (solid curve), 4-bit pulse compression (dashed curve), and 8-bit pulse compression (dotted-dashed curve) during 0130–0330 LT on June 19, 1999.

5.3 *Preliminary observations of wind velocity variations associated with the typhoon*

Figure 9 shows the time-height cross-section of zonal-meridional wind velocities averaged every 30 min obtained by the LTR between 18 LT on July 7 and 09 LT on July 8, 2000. Rain was observed at the MU Observatory during 00–03 LT on July 8. The LTR can continuously provide the data up to about 6 km without influence of weather conditions. Particularly, wind velocities up to 9–10 km are obtained on July 7, in spite of no rain on the ground. Figure 10 shows a weather chart at 03 LT on July 8, 2000. Typhoon 0003 (Kirogi) passed south of the radar site. A drastic change of wind velocities associated with the passage of the typhoon was observed with the LTR. Detailed analysis of these meteorological phenomena is beyond the scope of this paper. We will present detailed analysis results in subsequent papers.

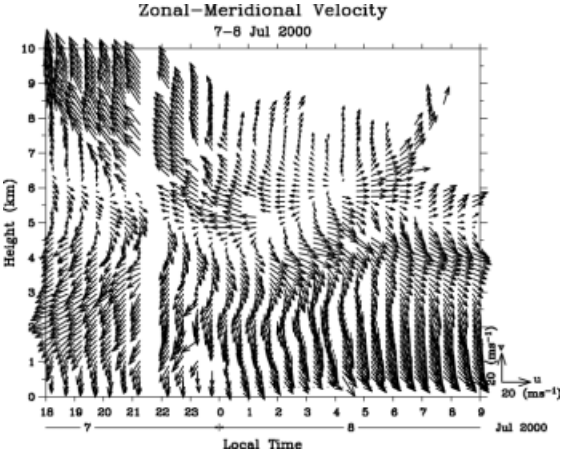

Fig. 9. Time-height cross-section of zonal-meridional wind velocities averaged every 30 min obtained by the LTR between 18 LT on July 7 and 09 LT on July 8, 2000.

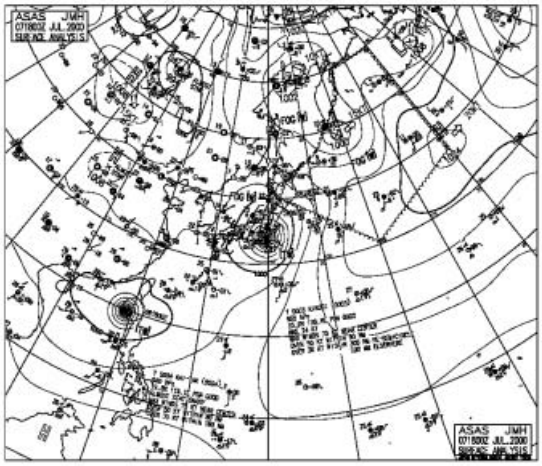

Fig. 10. Weather map at 03 LT on July 8, 2000.

6. LTR/RASS system

Temperature is one of the most important atmospheric parameters to clarify the structure of atmospheric phenomena. RASS (Radio Acoustic Sounding System) is a remote sensing technique to measure the height profiles of the virtual temperature by using acoustic transmitters and a pulse Doppler radar to detect the velocity of acoustic wavefronts. In this section, we describe the development of the LTR/RASS system and evaluate its performance.

First, we briefly review the principle of the RASS technique. Acoustic pulses transmitted from the ground produce refraction index fluctuations aloft, which scatter incident radio waves. We can detect the Doppler shift between the transmitted and received radio frequencies in the scattered radio waves, which we call RASS echoes, and can determine the propaga-

tion speed of acoustic wavefronts. In the real atmosphere, the apparent acoustic velocity $\vec{c_s}$ is the sum of the true acoustic velocity $\vec{c_a}$ and the background wind velocity $\vec{v_r}$.

$$\vec{c_s} = \vec{c_a} + \vec{v_r}. \tag{1}$$

Then, the acoustic velocity c_s measured by a radar becomes

$$c_s = \vec{c_s} \cdot \vec{n} = \vec{c_a} \cdot \vec{n} + \vec{v_r} \cdot \vec{n}, \tag{2}$$

where $\vec{n}$ is a unit vector parallel to the radar beam direction, and the dot $(\cdot)$ indicates an inner product. Meanwhile, virtual temperature T_v [K] can be derived by the acoustic velocity c_a [m s^{-1}] as

$$c_a = 20.047\sqrt{T_v}. \tag{3}$$

Using these principles, we can estimate the virtual temperature by RASS observations.

6.1 System requirements

The LTR/RASS system was designed to meet the following requirements:

1. It should be able to estimate the temperature within an accuracy of 0.5 K.
2. It should have a time resolution of a few minutes.
3. It should be sensitive enough to observe temperature profiles up to 1.5–2.0 km height under normal wind conditions.

The Bragg condition must be satisfied to obtain significant RASS echoes with a monostatic Doppler radar. It is expressed as

$$\vec{k_a} = 2\vec{k_e}, \tag{4}$$

where $\vec{k_a}$ and $\vec{k_e}$ are the acoustic and radio wavenumbers, respectively. Namely, the Bragg condition requires that the acoustic wavefronts must be normal to the beam direction, and that the acoustic wavelength must be half of the radar wavelength. Since the radar wavelength of the LTR is about 0.22 m, the wavelength of the acoustic wave is determined to be about 0.11 m, which corresponds to about 3 kHz in frequency.

Since we required the acoustic signal to include frequency components satisfying the Bragg condition in the measurement height range, we decided to sweep the frequency within the pulse length (e.g., Adachi et al. 1993; Masuda et al. 1992). It is expected that the maximum and minimum temperatures observed with LTR/RASS in Japan are about 30°C (which is the temperature near the ground in summer) and about −20°C (which is the temperature at the top of the ABL in winter), respectively. Therefore, the required frequency range for transmitted acoustic wave with the LTR/RASS is determined to be 2,886–3,159 Hz.

The frequency bandwidth of Doppler spectra obtained by the LTR is determined by the IPP and the number of coherent integrations. Since the RASS echoes have the Doppler velocity shift of 320–350 m s^{-1}, a wide frequency bandwidth is necessary to obtain the RASS echoes without frequency aliasing. It means that the IPP must be very short, and the number of coherent integrations must be very few. In order to improve velocity resolution, the number of FFT points must be very large to maintain the maximum velocity of 350 m s^{-1}. It is inefficient to satisfy both requirements, because of the reduction in S/N and the large amount of calculation. Therefore, we decided to employ the idea of shifting the receiving frequency from the transmitting frequency by about 3 kHz, which corresponds to an acoustic velocity of 331 m s^{-1} at 0°C. For the LTR system, it is possible to shift the frequency of the coherent oscillator (COHO) in the detector (see Fig. 1).

When the Bragg condition $\vec{k_a} = 2\vec{k_e}$ is satisfied, the received echo power P_r is theoretically described as (Adachi 1996)

$$P_r = \left(\frac{77.6 \times 10^{-8} p(r) r}{T(r)\gamma}\right)^2 \frac{4\pi^2 P_t}{\lambda^2 r^2} \left(\frac{\Delta r}{2}\right)^2, \tag{5}$$

where $p(r)$ and $T(r)$ are sound pressure and temperature, respectively, at range r, γ is the specific heat ratio, P_t is transmitting power, and Δr is a range resolution, respectively. By substituting $T = 275$ K, $P_t = 2$ kW, $\lambda = 0.22$ m, $\Delta r = 100$ m, and $P_r = -125$ dBm, which is the minimum detectable power considering the effect of integrations and Fourier transform, into (5), we can obtain $p(r) = 1.38 \times 10^{-4}$ W m^{-2}. On the other hand, the acoustic wave attenuates in the atmosphere, and the acoustic intensity $I = p^2/(\rho c_a)$ (where ρ is the atmospheric density) at range r is given by

$$I(r) = I(r_0) \exp(-\alpha r), \tag{6}$$

where α is the attenuation coefficient, which is related to the atmospheric temperature, pres-

sure, humidity, and acoustic frequency (Evans et al. 1972). The attenuation of $I(r)$ at 3 kHz is estimated as about 3.3 dB/100 m at the height of 1 km (890 hPa), the temperature of 20°C, and the relative humidity of 30% (Crocker 1998). The attenuation varies with atmospheric parameters and strongly depends on relative humidity (for example 8.3 dB/100 m and 1.5 dB/100 m for the relative humidity of 10% and 100%, respectively, at 1 km and 20°C). Assuming the constant attenuation of 3.3 dB/100 m, we need a transmitting acoustic pressure of at least 0.32 W m^{-2} (115 dB) for the maximum observable height of 2 km.

According to the MU radar/RASS experiments, it has been found that the height coverage is significantly reduced under strong wind conditions. Masuda (1988) employed ray-tracing in order to analyze the propagation characteristics of acoustic wavefronts, and showed that the normal condition depends largely on profiles of background temperature and horizontal wind velocity, as well as distance between radar and acoustic sources. In the case of LTR/RASS observations, the LTR cannot always steer the beam in the windward direction, while the MU radar can. If the wind flows from the direction to which the LTR cannot steer the beam, it is expected that the height coverage is severely reduced. Based on the discussions using ray-tracing of acoustic wavefronts for various wind conditions (Masuda 1988), we decided on the speaker positions as shown in Fig. 11. Because one of the requirements for LTR is the transportability, the number of speakers should be as few as possible. Thus, we use eight speakers.

6.2 *Acoustic transmitters*

We have developed the acoustic transmitters for the LTR/RASS based on the discussion in the previous subsection. The horn speakers must be portable and compact enough to be placed around the LTR antenna. Therefore, we decided to employ a hyperbolic horn speaker, which is a typical acoustic horns.

The designed horn speaker system consists of a hyperbolic horn and a loudspeaker unit. With regard to the material of the horn, we chose wooden boards to avoid vibration due to intense acoustic pressure. The maximum sound pressure level is 131 dB (12.6 W m^{-2}), according to the specification of the compression driver (JBL 2450H). Therefore, the maximum observable height of the LTR/RASS is estimated at about 2.4 km under ideal wind conditions. A picture of the horn speaker system is shown in Fig. 12. The horn surface is coated with silicon to prevent it from rotting. The horn is mounted on a frame with wheels, and is fixed by concrete blocks in order to prevent it moving in a strong wind.

The original acoustic wave is generated by the sound device controlled by the software in the workstation, and it is transferred to the sound device (YAMAHA, DS-2416) loaded in the personal computer for controlling the

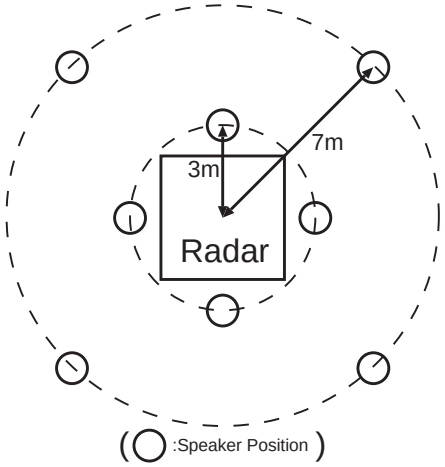

Fig. 11. Speaker positions for LTR/RASS.

Fig. 12. Picture of a hyperbolic horn speaker system. The horn is mounted on a frame with wheels.

acoustic signals through the audio cable. After reducing the noise due to the cable, it is amplified and distributed to eight lines in the sound device by the software operated in the personal computer. Then, the acoustic waves are transferred to the power amplifiers (Amcron, MA-601) through the audio cables. Because each power amplifier can amplify two acoustic signals independently, we use four power amplifiers.

6.3 Software system

We must control the acoustic waves and acoustic transmitters in RASS observations. The block diagram of software for RASS observations is indicated in Fig. 4. The 'Sound Control' and the 'Device Control' are new programs for RASS observations. The 'Sound Control' program has the functions of generating acoustic signals and controlling the acoustic signal transmission. 'RASS-PC' in this figure is a personal computer for loading 'Sound Device', which is the sound device to amplify and distribute the acoustic signals. The 'Device Control' program is operated in 'RASS-PC' and has the function of controlling the sound device.

In the RASS observation mode, the 'Sound Control' program is executed by the 'Data Transfer' program. Since the acoustic wave is much slower than the radio wave, the radio wave must be transmitted after the acoustic wave reaches the observation height. The 'Sound Control' program calculates the current observation time and starts to transmit the acoustic signals 10 s before the start of the RASS observation, then it periodically transmits acoustic signals every 5 s, until the end of the RASS observation. Because the length of the acoustic signal is about 1 s, the time interval is determined by considering the load of the power amplifier and horn speakers.

The 'Device Control' program is always operated in 'RASS-PC', and periodically reads the 'control' file in the workstation through the network. Operators write which speaker transmits acoustic waves and the attenuation level of acoustic waves into the 'control' file. The 'Device Control' program opens or closes the output lines and attenuates transmitting acoustic wave according to the 'control' file. Then, it writes the current status of each speaker to the 'status' file in the workstation. By making a comparison between 'control' and 'status' files, operators can confirm that the 'Device Control' program is operating correctly, which means that acoustic waves are being correctly transmitted.

On the other hand, because the receiving frequency is shifted by 3 kHz in RASS observations, ground clutter echoes are frequency aliased and do not appear at the center of the Doppler spectrum data. In addition, the position of ground clutter echoes in the spectrum varies with the observation parameters, which are chosen to separate the RASS echoes from the ground clutter and the clear-air echoes. Furthermore, the frequency offset between two COHOs is not always exactly 3 kHz and has a long-term drift within $\pm$100 Hz. Because the center of the Doppler spectrum corresponds to the frequency offset, it is necessary to know the frequency offset accurately to estimate the Doppler shift of RASS echoes. We can estimate the frequency offset accurately from the position of ground clutter echoes, which always appear at the zero Doppler component, although we have to take frequency aliasing into account. Therefore, the fitting method for the RASS observation mode becomes the following procedure.

1. The frequency offset is calculated from the position of ground clutter echoes in the Doppler spectrum as follows: First, a frequency that clutter echoes should fold into the Doppler spectrum is calculated. It depends on the IPP and the number of coherent integrations (in the case of the parameters shown in Table 5, it is 2,500 Hz (275 m s^{-1})).

Table 5. Observation parameters of the LTR/RASS observations on December 11, 1999.

Parameter	Value
Inter-pulse period (IPP)	25 μs
Sub-pulse width	0.67 μs
Number of coherent integrations	32
Number of FFT points	512
Number of incoherent integrations	30
Number of beam directions	5
Zenith angle	9.8°
Number of sampling points	28
Pulse compression	no compression

A spectral peak is searched within $\pm$10 Hz ($\pm$1.1 m s^{-1}) around that frequency, and the first moment is calculated by the moment method using 10 spectral data points around the peak position in each range gate. Then, the median value of the first moment data in all the range gates is regarded as the frequency offset, taking into account frequency aliasing.

2. The spectral part in which ground clutter echoes do not appear is extracted from the Doppler spectrum, and the spectral parameters of RASS echoes are estimated.

The 'Signal Processing' program automatically selects the suitable method according to the observation mode.

6.4 *Preliminary observations and comparison with radiosonde measurements*

We conducted RASS observations on December 11, 1999. The LTR was operated alternately in wind and RASS observation modes, and background winds were compensated for measured acoustic velocity. Table 5 shows the observation parameters. The observation parameters of these two observation modes are the same. The IPP and number of coherent integrations were chosen so as not to superimpose the aliased ground clutter echoes and the clear air echoes on the RASS echoes. The range resolution is 100 m. The resolution of line-of-sight velocity is 0.27 m s^{-1}, which corresponds to the resolution of virtual temperature of 0.45 K at 0°C. Because the observation time of each observation mode is about 1 min, the time resolution of the virtual temperature profiles is about 2 min. In order to verify the accuracy of the virtual temperature obtained by the LTR/RASS, we launched the radiosonde at the radar site.

Figure 13 shows a comparison of the virtual temperature profiles between LTR/RASS and radiosonde results. The standard deviations of the RASS results are indicated by the horizontal bars. The launch time of the radiosonde was 2050 LT, and the LTR/RASS profiles were averaged over 30 min during 2050–2120 LT. The virtual temperature of both results are in good agreement. The mean difference does not exceed 0.6 K from 100 m up to 600 m heights. On the other hand, the mean difference reaches about 1 K at about 1 km height, and the standard deviation is much larger than that for lower heights. Therefore, the maximum observation height in this case is about 600 m, which is lower than the height expected in Subsection 6.1. Observations were carried out on a stormy winter's day, with strong winds. The horizontal wind velocity at ground level observed by anemometer was about 4 m s^{-1}, and that at 1 km observed by the LTR was 15 m s^{-1} in a southeasterly direction. Therefore, it is considered that the acoustic wavefronts were blown by the background wind, and the RASS echoes could not be received by the LTR. Since we obtained the highest observable height of 600 m based on the discussion using ray-tracing with the observed wind profile, the observational results of LTR/RASS are reasonable. Under normal wind conditions, temperature observations up to 1.5–2.0 km are expected feasible. In the above case in the clear-air, we compensated the effect of background winds for measured acoustic velocity. We have to note in the rainy case that background winds cannot be correctly compensated, since precipitation echoes are dominant.

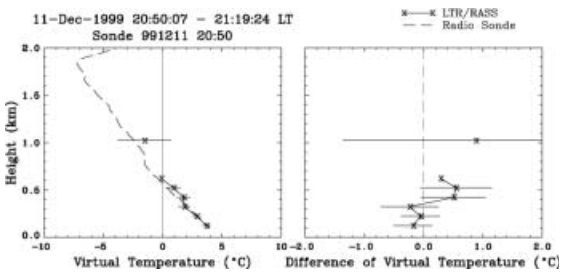

Fig. 13. Left panel shows virtual temperature profiles with LTR/RASS (solid curve with cross signs) averaged over 2050–2120 LT on December 11, 1999 and with radiosonde (dashed curve) launched at 2050 LT. Right panel shows the difference of virtual temperature between RASS and radiosonde. Horizontal bars indicate standard deviation of RASS results for 30 min.

7. Concluding remarks

In this study, we have developed a Lower Troposphere Radar (LTR) which is the first active phased-array type wind profiler in the 1.3-GHz band. The antenna gain of 33 dBi

is obtained by developing a 4 m × 4 m active phased array antenna, which has 96 antenna sub-elements. The peak output power of 2 kW is obtained by using 24 active transmitting modules. S/N is improved up to 8 times by using a pulse compression technique which uses 8-bit Spano and Ghebrebrhan's coding. Three-dimensional atmospheric wind data are obtained with high time and height resolutions in real time. We showed simultaneous observation results with the MU radar and the Doppler sodar, and have confirmed LTR's potential as a reliable tool for observations of wind velocity profiles in the lower troposphere, including the atmospheric boundary layer. Evaluation of pulse compression was discussed, and the effect of the pulse compression was well shown. Detailed observations and numerical model studies may be expected by using this radar.

We also described the LTR/RASS system. We designed the acoustic transmitters and discussed the transmitting acoustic waves to satisfy the Bragg condition at different heights. Eight hyperbolic horn speakers were arranged to observe up to 1.5–2.0 km under normal wind conditions. We showed the initial results of the virtual temperature profile obtained by LTR/RASS observations, and the comparison with a radiosonde sounding, although we need more comparisons to verify their accuracy.

The LTR is now continuously operated at the Shigaraki MU Observatory in standard wind observation mode. In March 2001, the Japan Meteorological Agency (JMA) installed their 'Wind Profiler Network' (WINDAS), which consists of 25 LTRs[3], covering Japan. Because the LTR has the advantage of being able to observe wind profiles with high time and height resolutions, we expect that it will contribute to the improvement of weather prediction. One important application of the LTR is to mount it on a ship to observe the atmospheric dynamics over the sea (Law et al. 2002). To compensate in real time for the roll and pitch of the ship, the beam direction can be electrically controlled since the LTR enables fast beam steering. We will present its observing system and observation results in subsequent papers.

3 Six LTRs are added in WINDAS in 2003.

Acknowledgments

We thank Prof. T. Tsuda, Prof. T. Sato, Dr. M. Yamamoto, and Dr. T. Nakamura for numerous technical comments on the development of the LTR. We thank Dr. J. Furumoto for technical comments on the development of the LTR/RASS. We thank Dr. T. Hayashi and Dr. Y. Ito for providing the Doppler sodar data. We thank Dr. Gernot Hassenpflug for his careful reading of the original manuscript. Thanks are also due to the anonymous reviewer and the editor (Prof. Y. Fujiyoshi) for their constructive comments. The MU radar belongs to and is operated by Radio Science Center for Space and Atmosphere of Kyoto University. The present study was financially supported by Grants-in-Aids (10354007) of the Japan Society for the Promotion of Science (JSPS).

References

Adachi, A. and T. Kobayashi, 2001: RHI observation of precipitation with boundary layer wind profiler, *30th international conference on radar meteorology*, 116–117.

Adachi, T., 1996: *Detailed temperature structure of meteorological disturbances observed with RASS (Radio Acoustic Sounding System)*, Ph.D Thesis, Kyoto University, Japan, pp. 171.

———, T. Tsuda, Y. Masuda, T. Takami, S. Kato, and S. Fukao, 1993: Effects of the acoustic and radar pulse length ratio on the accuracy of radio acoustic sounding system (RASS) temperature measurements with monochromatic acoustic pulses, *Radio Sci.*, **28**, 571–583.

Carter, D.A., K.S. Gage, W.L. Ecklund, W.M. Angevine, P.E. Johnston, A.C. Riddle, J. Wilson, and C.R. Williams, 1995: Developments in UHF lower tropospheric wind profiling at NOAA's Aeronomy Laboratory, *Radio Sci.*, **30**, 977–1001.

Crocker, M.J., 1998: *Handbook of Acoustics*, John Wiley & Sons, Inc., New York.

Ecklund, W.L., D.A. Carter, and B.B. Balsley, 1988: A UHF wind profiler for the boundary layer: Brief description and initial results, *J. Atmos. Oceanic Technol.*, **5**, 432–441.

———, ———, ———, P.E. Currier, J.L. Green, B.L. Weber, and K.S. Gage, 1990: Field tests of a lower tropospheric wind profiler, *Radio Sci.*, **25**, 899–906.

Evans, L.B., H.E. Bass, and L.C. Sutherland, 1972: Atmospheric absorption of sound: Theoretical predictions, *J. Acoust. Amer.*, **51**, 1565–1575.

Fukao, S., T. Sato, T. Tsuda, S. Kato, K. Wakasugi, and T. Makihira, 1985a: The MU radar with an active phased array system, 1. Antenna and power amplifiers, *Radio Sci.*, **20**, 1155–1168.

———, T. Tsuda, T. Sato, S. Kato, K. Wakasugi, and T. Makihira, 1985b: The MU radar with an active phased array system, 2. In-house equipment, *Radio Sci.*, **20**, 1169–1176.

———, K. Wakasugi, T. Sato, S. Morimoto, T. Tsuda, I. Hirota, I. Kimura, and S. Kato, 1985c: Direct measurement of air and precipitation particle motion by very high frequency Doppler radar, *Nature*, **316**, 712–714.

———, T. Sato, T. Tsuda, M. Yamamoto, M.D. Yamanaka, and S. Kato, 1990: MU Radar: New capabilities and system calibrations, *Radio Sci.*, **25**, 477–485.

Gaynor, J.E., 1994: Accuracy of sodar wind variance measurements, *International Journal of Remote Sensing*, **15**, 313–324.

Hadi, T.W., T. Tsuda, H. Hashiguchi, and S. Fukao, 2000: Tropical sea-breeze circulation and related atmospheric phenomena observed with *L*-band boundary layer radar in Indonesia, *J. Meteor. Soc. Japan*, **78**, 123–140.

Hashiguchi, H., M.D. Yamanaka, T. Tsuda, M. Yamamoto, T. Nakamura, T. Adachi, S. Fukao, T. Sato, and D.L. Tobing, 1995a: Diurnal variations of the planetary boundary layer observed with an *L*-band clear-air Doppler radar, *Bound.-Layer Meteor.*, **74**, 419–424.

———, S. Fukao, T. Tsuda, M.D. Yamanaka, D.L. Tobing, T. Sribimawati, S.W.B. Harijono, and H. Wiryosumarto, 1995b: Observations of the planetary boundary layer over equatorial Indonesia with an *L*-band clear-air Doppler radar: Initial results, *Radio Sci.*, **30**, 1043–1054.

———, ———, M.D. Yamanaka, T. Tsuda, S.W.B. Harijono, and H. Wiryosumarto, 1995c: Boundary layer radar observations of the passage of the convection center over Serpong, Indonesia (6°S, 107°E) during the TOGA COARE intensive observation period, *J. Meteor. Soc. Japan*, **73**, 535–548.

———, ———, T. Tsuda, M.D. Yamanaka, S.W.B. Harijono, and H. Wiryosumarto, 1996: An overview of the planetary boundary layer observations over equatorial Indonesia with an *L*-band clear-air Doppler radar, *Contr. Atmos. Phys.*, **69**, 13–25.

———, ———, M.D. Yamanaka, and T. Tsuda, 1997: Frequency spectra of wind velocity fluctuations between 1 hour and 1 month in the atmospheric boundary layer over equatorial Indonesia, *J. Geomag. Geoelectr.*, **49**, S187–S195.

Ishihara, M. and H. Goda, 2000: Operational 1.3 GHz-wind profiler network of Japan Meteorological Agency, *Proceedings of the Ninth International Workshop on Technical and Scientific Aspects of MST Radar, Toulouse, March 13–18, 2000*, 538–540.

Ito, Y., 1997: Errors in wind measurements estimated by five-beam phased array Doppler sodar, *J. Atmos. Oceanic Technol.*, **14**, 792–801.

Kato, Y., T. Abo, K. Kobayashi, Y. Izumikawa, and M. Ishihara, 2004: The wind profiler network of the Japan Meteorological Agency, *Tenki*, **50**, 891–907 (in Japanese).

Law, D.C., S.A. McLaughlin, M.J. Post, B.L. Weber, D.C. Weksh, and D.E. Wolfe, 2002: An electronically stabilized phased array system for shipborne atmospheric wind profiling, *J. Atmos. Oceanic Technol.*, **19**, 924–933.

Masuda, Y., 1988: Influence of wind and temperature on the height limit of a radio acoustic sound system, *Radio Sci.*, **23**, 647–654.

———, J. Awaka, K. Nakamura, T. Adachi, and T. Tsuda, 1992: Analysis of the radio acoustic sounding system using a chirped acoustic wave, *Radio Sci.*, **27**, 681–691.

May, P.T., T. Adachi, T. Tsuda, and R.J. Lataitis, 1996: The spatial structure of RASS echoes, *J. Atmos. Oceanic Technol.*, **13**, 1275–1290.

Miyashita, H., H. Ohmine, K. Nishizawa, S. Makino, and S. Urasaki, 1999: Electromagnetically coupled coaxial dipole array antenna, *IEEE Trans. Antennas Propagat.*, **47**, 1716–1726.

Ohno, Y., 1995: Land and sea breezes observed by a 1357 MHz wind profiler, *Proceedings of the Seventh Workshop on Technical and Scientific Aspects of MST Radar, South Carolina, November 7–11, 1995*, 323–326.

Reddy, M.C., A.K. Ghosh, V.S. Kumar, A.R. Jain, T. Kozu, and K.K. Reddy, 2000: Integrated measurements of atmospheric winds using Indian MST radar and lower atmospheric wind profiler (LAWP), *Proceedings of the Ninth International Workshop on Technical and Scientific Aspects of MST Radar, Toulouse, March 13–18, 2000*, 222–225.

Schmidt, G., R. Ruster, and P. Czechowsky, 1979: Complementary code and digital filtering for detection of weak VHF radar signals from the mesosphere, *IEEE Trans. on Geosci. and Remote Electron.*, **17**, 262–280.

Spano, E. and O. Ghebrebrhan, 1996a: Pulse coding techniques for ST/MST radar systems: A general approach based on a matrix formulation, *IEEE Transactions on Geoscience and Remote Sensing.*, **34**, 304–316.

——— and ———, 1996b: Complementary sequences with high sidelobe suppression factors for ST/MST radar applications, *IEEE Transactions on Geoscience and Remote Sensing.*, **34**, 317–329.

——— and ———, 1996c: Sequences of complementary codes for the optimum decoding of truncated ranges and high sidelobe suppression factors for ST/MST radar systems, *IEEE Transactions on Geoscience and Remote Sensing.*, **34**, 330–345.

Tsuda, T., S. Fukao, M. Yamamoto, T. Nakamura, M.D. Yamanaka, T. Adachi, H. Hashiguchi, N. Fujioka, M. Tsutsumi, S. Kato, S.W.B. Harijono, T. Sribimawati, B.P. Sitorus, R.B. Yahya, M. Karmini, F. Renggono, B.L. Parapat, W. Djojonegoro, P. Mardio, N. Adikusumah, H.T. Endi, and H. Wiryosumarto, 1995: A preliminary report on observations of equatorial atmosphere dynamics in Indonesia with radars and radiosondes, *J. Meteor. Soc. Japan*, **73**, 393–406.

Wakasugi, K., A. Mizutani, M. Matsuo, S. Fukao, and S. Kato, 1986: A direct method for deriving drop-size distribution and vertical air velocities from VHF Doppler radar spectra, *J. Atmos. Ocean. Tech.*, **3**, 623–629.

———, ———, ———, ———, and ———, 1987: Further discussion on deriving drop-size distribution and vertical air velocities directly from VHF Doppler radar spectra, *J. Atmos. Ocean. Tech.*, **4**, 170–179.

Widiyatmi, I., M.D. Yamanaka, H. Hashiguchi, S. Fukao, T. Tsuda, S. Ogino, S.W.B. Harijono, and H. Wiryosumarto, 1999: Quasi 4 day mode observed by a boundary layer radar at Serpong (6°S, 107°E), Indonesia, *J. Meteor. Soc. Japan*, **77**, 1177–1184.

———, H. Hashiguchi, S. Fukao, M.D. Yamanaka, S. Ogino, K.S. Gage, S.W.B. Harijono, S. Diharto, and H. Djojodihardjo, 2001: Examination of 3–6 day disturbances over equatorial Indonesia based on boundary layer radar observations during 1996–1999 at Bukittinggi, Serpong, and Biak, *J. Meteor. Soc. Japan*, **79**, 317–331.

Woodman, R.F., 1980: High-altitude resolution stratospheric measurements with the Arecibo 430-MHz radar, *Radio Sci.*, **15**, 423–430.